Implementation of Broadband Electrically Detected Magnetic Resonance in a Sub-THz FraScan Spectrometer

Artur Solodovnyk, Dariya Savchenko, Oleksii Laguta, and Petr Neugebauer

***Abstract*— Electrically detected magnetic resonance (EDMR) is an effective spectroscopic method used for characterizing semiconductive solid-state materials. High spin sensitivity and the capability to explore spin-dependent transport mechanisms, which are crucial for the development of semiconductor devices, define it from other methods based on magnetic resonance. High frequency and high magnetic field EDMR implementation was motivated by the necessity to obtain access to more precise, high-resolution data to enhance the method's research potential. We present an EDMR system based on a unique THz FraScan spectrometer, which performs frequency sweeps ranging from 80 GHz to 1.1 THz, and the magnetic field sweeps up to 16 T. The study addresses the instrumentation, detection scheme, and 85–328.84-GHz EDMR results on highly nitrogen-doped 15R SiC monocrystals. Furthermore, the results demonstrate a subjective advantage of frequency-domain EDMR (FD EDMR) over conventional magnetic field domain measurements in terms of substantially greater signal-to-noise ratio (SNR) and the ability to record an EDMR frequency-field map (EDMR FFM).**

***Index Terms*— 15R SiC, electrically detected magnetic resonance (EDMR), frequency-domain EDMR (FD EDMR), magnetic resonance, SiC, sub-THz, THz.**

I. Introduction

THE magnetic resonance technique—electrically detected magnetic resonance (EDMR)—has been proven a sensitive (about 10^7 times greater than electron paramagnetic resonance (EPR) [1]) and powerful method for characterization of charge carriers, defects, and impurities in a variety of semiconductive solids by providing insights into fundamental physical phenomena of magnetic resonance and aid in situ studies for further reliable devices development [2], [3]. It is based on EPR but differs in its detection scheme: spin-dependent processes are monitored via the change in the device's current or voltage under the resonance microwave excitation. In EPR, the transitions between electron spin energy levels [see Fig. 1(a) and (b)] are measured as a microwave absorption, when the following resonance condition is fulfilled:

$$h\nu = g\mu_B B \tag{1}$$

where h is the Planck constant ($\mathrm{J} \cdot \mathrm{Hz}^{-1}$), ν is the microwave frequency (Hz), μ_B is the Bohr magneton ($9.274 \times 10^{-24}\ \mathrm{J} \cdot \mathrm{T}^{-1}$), g is the g-factor, and B is the magnetic field (T) [4]. It should be noted that (1) describes the simplest case of a system with spin $S = 1/2$ with the isotropic Zeeman interaction. The splitting of these energy levels in the presence of the magnetic field is called the Zeeman effect [see Fig. 1(a)]. In EDMR, these transitions are observed as a change in the electrical conductivity of the sample [see Fig. 1(a) and (c)]. The reasons causing this change are spin-dependent processes such as recombination, tunneling, or hopping [5], [6]. Unlike the EPR, which is not sensitive to these processes, EDMR can explore these transport mechanisms, considering that they are based on spin selection rules. The motivation for using detection of electrical conductivity, rather than the microwave absorption, results from the importance of point defects, and impurities in semiconductor devices. Their concentration in modern devices is too low for conventional EPR, which requires at least 10^{11} of paramagnetic centers, whereas the EDMR can be observed within 10^6 defects [7], [8].

This method's history began in 1960s. One of the first EDMR observations was in 1966, where Schmidt and Solomon [9] described spin-dependent recombination of free carriers, investigated in phosphorus-doped silicon. In 1972, Lepine [10] proposed that the capture of the conduction electron by the recombination center depends on their relative spin orientation. Problems developed when this model was unable to account for the signals observed in later measurements made by other researchers. There were several prior theoretical attempts to explain the EDMR signal before Kaplan et al. [11] turned to Pauli's permutation-symmetry model based on the Pauli blockade in 1978. According to the description, charge

Manuscript received 2 November 2022; revised 22 May 2023; accepted 26 May 2023. Date of publication 20 June 2023; date of current version 29 June 2023. This work was supported in part by the Internal Grant Agency, Central European Institute of Technology (CEITEC), Czech Republic, under Grant VUT-J-19-6070; in part by the Ministry of Education, Youth and Sports of the Czech Republic (MEYS CR) under Project CEITEC 2020 (LQ1601); in part by the CEITEC Nano Research Infrastructure, MEYS CR, under Grant LM2018110; and in part by the CEITEC Brno University of Technology. The work of Artur Solodovnyk and Petr Neugebauer was supported by the European Research Council (ERC) through the European Union's Horizon 2020 Research and Innovation Program under Grant 714850. The work of Dariya Savchenko was supported by the Operational Program Research, Development and Education financed by the European Structural and Investment Funds and the Czech Ministry of Education, Youth and Sports under Project SOLID21 CZ.02.1.01/0.0/0.0/16_019/0000760. The work of Oleksii Laguta was supported by the Grant Agency of the Czech Republic under Grant EXPRO: 21-20716X. The Associate Editor coordinating the review process was Dr. Alessio De Angelis. *(Corresponding author: Petr Neugebauer.)*

Artur Solodovnyk was with the Central European Institute of Technology, Brno University of Technology, 612 00 Brno, Czech Republic. He is now with the Department of Engineering Science and Mechanics, The Pennsylvania State University, State College, PA 16802 USA (e-mail: abs7141@psu.edu).

Dariya Savchenko is with the Institute of Physics, Czech Academy of Sciences (CAS), 182 21 Prague, Czech Republic, and also with the Department of General Physics and Modeling of Physical Processes, National Technical University of Ukraine "Igor Sikorsky Kyiv Polytechnic Institute," 03056 Kyiv, Ukraine.

Oleksii Laguta and Petr Neugebauer are with the Central European Institute of Technology, Brno University of Technology, 612 00 Brno, Czech Republic (e-mail: petr.neugebauer@ceitec.vutbr.cz).

This article has supplementary downloadable material available at https://doi.org/10.1109/TIM.2023.3284951, provided by the authors.

Digital Object Identifier 10.1109/TIM.2023.3284951

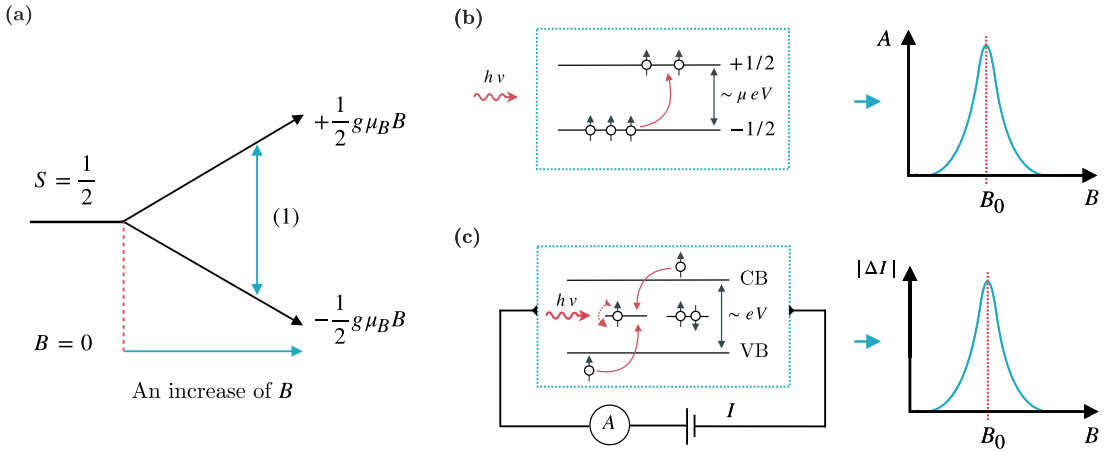

Fig. 1. (a) Diagram of the Zeeman effect for a system with spin $S = 1/2$ (case, which includes only the isotropic Zeeman interaction) placed in the magnetic field B; h is the Planck constant, ν is the microwave frequency, μ_B is the Bohr magneton, and g is the g-factor. (b) Basic principle of EPR detection. The EPR transition in the sample due to the resonance condition (1) is observed as the microwave absorption of the sample. (c) Principle of EDMR detection. Microwave irradiation flips the spin of the unpaired electron in the defect center (recombination center) and the spin-dependent process happens. As a result, one observes a change in the sample current under the resonance condition (1). Note that a common Zeeman energy splitting is in a range of μeV, whereas the bandgap in the semiconductor is in eV.

TABLE I

SHORT COMPARISON OF EXISTING EDMR RESEARCH SETUPS. MD—MAGNETIC FIELD DOMAIN (MAGNETIC FIELD SWEEP, CONSTANT FREQUENCY), FD—FREQUENCY DOMAIN (FREQUENCY SWEEP, CONSTANT MAGNETIC FIELD), CW—CONTINUOUS WAVE

Research field	Methods used	Setup type	Frequency range (GHz) / Magnetic field max (T)	References
Solar cells	Conventional CW and pulse modes	Commercial X-, Q-band and 263 GHz	10, 35, 263 / 1.2, 9	[13]
Wafer-based devices	CW MD and FD, Rapid Scan	Homebuilt low frequency (< 500 MHz), X-Band, Wafer-probing station	< 0.5, 10 / 0.1, 1	[19]–[22]
Quantum computing	CW and pulse	Commercial X-band	10 / 1	[23]–[26]
General	CW and pulse	Heterodyne Quasi-Optical spectrometer	120–336 / 12.5	[27], [28]
General (Current work)	CW MD and FD, Rapid Scan	Homebuilt THz FraScan spectrometer	80–1100 / 16	[15], [17]

carriers in localized electronic states first form an "exceptional pair" during a "readjustment time" before a recombination transition happens. A more thorough explanation of EDMR, as well as a detailed description of several spin-dependent models, can be found elsewhere [5], [6].

Commonly, the EDMR setups are built using commercial EPR spectrometers with applied hardware and software modifications [12], [13], [14]. Consequently, the microwave frequency and the magnetic field range are defined by the vendor in EPR spectrometers for their particular application (e.g., commercially standardized X-band in CW and pulse modes, see Table I). Thereby, the EDMR capabilities directly depend on the EPR setup itself. This work describes the development of an EDMR setup based on the THz FraScan EPR spectrometer (located in Central European Institute of Technology (CEITEC), Brno, Czech Republic) which works within the frequency range of 80–1100 GHz and in magnetic fields up to 16 T [15]. The urge to have the possibility to perform studies using higher frequencies and higher magnetic fields paves a way to access higher spin polarization, higher g-factor resolution, large zero-field splitting, etc., which among others provides more accurate and high-resolution data [13], [16], [17], [18]. Among the exceeding amount of EDMR applications, we can highlight the following:

1) solar cells research [13], [29], [30];
2) MOSFET, nano-scale transistors, device reliability research (irradiation damage, high electric field stressing) [19], [20], [31];
3) quantum computing, electronic spin storage, write/readout [23], [24], [25], [26].

Using our THz FraScan spectrometer, we demonstrate the implementation of the EDMR technique in high magnetic fields and high frequencies to broaden the existing technique's research possibilities. The setup's functionality is demonstrated using EDMR measurements on highly nitrogen-doped 15R SiC monocrystals. Section II describes the experimental setup, the EDMR detection scheme, and the sample holder.

II. EXPERIMENTAL SETUP

Going for higher frequencies in EDMR using conventional EPR spectrometers is rather complicated already at the Q-band in terms of the space for the sample in the cavity, which is limited by 2 mm, at the W-band it is about a half of millimeter.

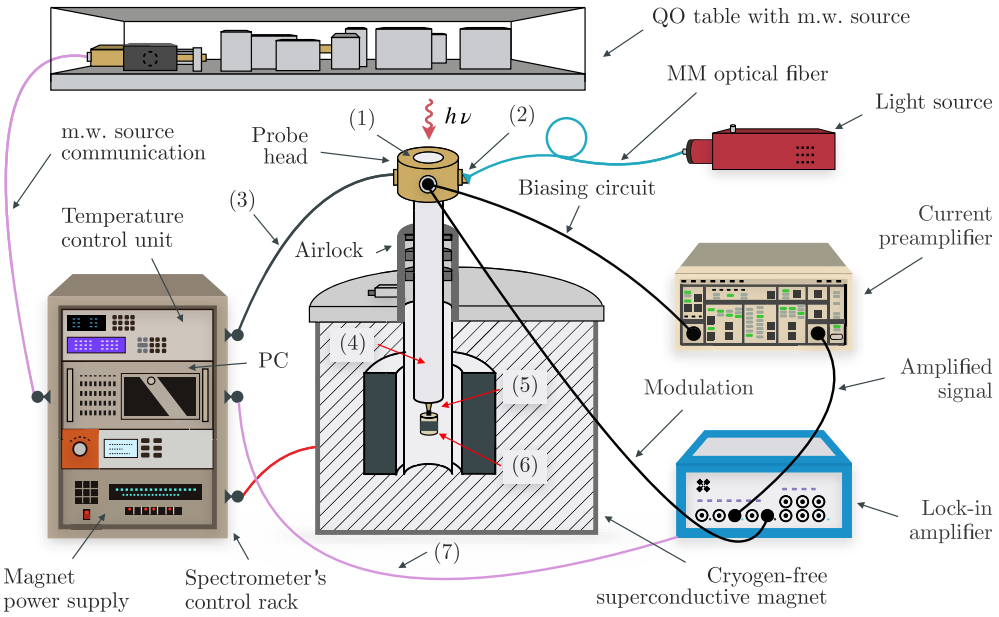

Fig. 2. General scheme of sub-THz EDMR setup. (1) Microwave window, (2) optical fiber feedthrough, (3) temperature and magnetic field sensors, (4) EPR probe, (5) variable temperature insert (VTI) space, (6) EDMR sample holder, and (7) lock-in amplifier communication. QO—quasi-optics, MM—multimodal, m.w.—microwave. Data cables are indicated in violet color, signal cables—black, power—red color.

Thus, it becomes more and more challenging to place a functioning device or a sample of working dimensions with increasing frequency. However, the THz FraScan spectrometer's nonresonant cavity-free configuration eliminates this issue. Apart from the setups that use microwave (m.w.) cavities, higher frequency ($>W$-band) solutions use quasi-optics (QO) for m.w. propagation. Some of the earliest nonresonant broadband systems for high-field EPR and EDMR can be found in [13], [17], [25], [32], and [33]. QO, in our case, is a set of instrumentation such as elliptical mirrors, absorbers, and Faraday rotators, for the free-space propagation of the THz-range Gaussian beam. Because the QO supports broadband operation, the frequency sweep option becomes possible. Fig. 2 depicts the general layout of an EDMR experiment. Quasi-optical m.w. bridge works in two modes: EPR and EDMR. A set of active and passive multipliers (Virginia Diodes Inc., Charlottesville, VA, USA) allow the gap-less generation of microwaves with the frequencies ranging from 80 GHz to 1.1 THz. To conduct the EPR experiment, both the m.w. sources and the m.w. detectors are used, the EDMR measurement though requires only the m.w. source. The microwaves from the QO m.w. bridge propagate inside of an oversized corrugated waveguide of the EPR probe and irradiate the sample placed in the holder, which is attached to the end of the probe. The EPR probe is placed inside a cryogen-free superconducting magnet system (16 T, Cryogenic Ltd., London, U.K.) so that the sample is located in the middle of the magnetic field. A home-built airlock prevents the system's contamination by air during inserting/extracting of the probe. For the majority of the experiments, the magnitude of magnetic field is read out from the magnet's power supply. For the precise determination of the magnetic field, a reference sample with a known g-factor should be used (in this work, we used Cr^{3+}:MgO ($g = 1.9797$) standard sample). In the variable temperature insert (VTI) space (5), the temperature can be varied from 300 K to 1.8 K (and can be measured precisely via a temperature sensor (3). The EPR probe head has three signal connectors and one optical fiber feedthrough (2), which allows to use different light sources (in this work, we used diode lasers with the wavelengths of 403–636.7 nm and the broadband SLS201L lamp (Thorlabs, Inc., Newton, NJ, USA)) for the EDMR experiment. Also, it contains an m.w. window made of Mylar foil (thickness of $\approx$70 μm), which isolates the VTI highly pure He atmosphere from the ambient air.

A common EDMR experiment requires the detection of extremely small changes in electric current in the pA range, and for this reason we use an SR570 (Stanford Research Systems Inc., Sunnyvale, CA, USA) current preamplifier. Depending on the sample's required bias voltage, the different biasing source can be used. However, to avoid additional noise pickups, we used the SR570's internal circuitry, which provides the biasing voltage of $-5\cdots+5$ V. In addition, we use a phase-sensitive detection (PSD) approach to substantially improve the signal-to-noise ratio (SNR) [34]. For the PSD method, we use the magnetic field modulation, created by a small coil around the sample, as shown in Section III. The amplified signal from the sample is demodulated via an MFLI-500KHz (Zurich Instruments Ltd., Zürich, Switzerland) lock-in amplifier, and a home-written LabVIEW program controls spectrometer's equipment and acquires the EDMR signal from the lock-in amplifier. To the end of the EPR probe, we attach the EDMR sample holder, which is described in Section III.

III. Sub-THz EDMR Sample Holder

The materials for the sample holder (see Fig. 3) were chosen based on the given conditions for a high magnetic field and a low-temperature environment. The body of the sample holder and the inner base were made of polyether ether

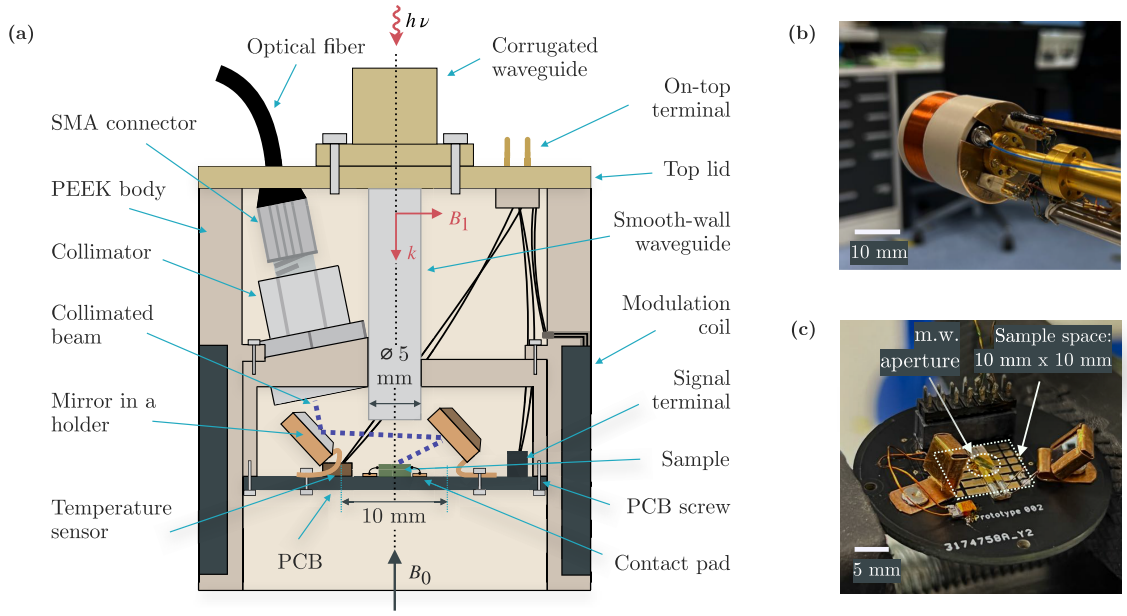

Fig. 3. (a) Schematic illustration of the EDMR sample holder. The direction of the magnetic field B_0 and m.w. beam described by the propagation vector k and the corresponding B_1 field are indicated in the illustration. (b) Sample holder is attached to the corrugated waveguide. (c) PCB with mirrors and the sample. The allowed sample dimensions in this configuration are 10 × 10 × 7 mm ($L \times W \times H$), and the microwave aperture is 5 mm in diameter.

ketone (PEEK), which is a colorless organic thermoplastic polymer in the polyaryletherketone (PAEK) family, widely used in engineering applications. This material is able to withstand such extreme conditions. A commercial optical fiber collimator 300051 (World Precision Instruments Inc., Sarasota, FL, USA) uses a nonmagnetic stainless steel shell; the mirror holders were manufactured from a phosphor–bronze sheet (thickness of 0.2 mm). Broadband square 5 mm mirror UV-enhanced aluminum-coated, $\lambda/10$ mirrors (Edmund Optics Inc., Barrington, NJ, USA) (250–700 nm) in Fig. 3(c) direct the light beam from the collimator to the sample. During cooldown and warmup of the VTI space, the light reflected from the mirrors has no significant sight of deviation (see Supplementary information). The sample is placed on a custom printed circuit board (PCB) with gold-plated copper electrical connections and FR-4 insulation (woven glass and epoxy) (see Supplementary information). Using a PCB as a sample plate has the advantage of having reliable electrical connections and also providing mechanical and thermal stability. For instance, in the "ambient" mode, when the microwave source and the current to the modulation coil are off, the difference in the temperature of VTI space and the sample can be less than 2 K; in the measurement mode, m.w. source and the modulation coil produce additional heat and the temperature difference can be up to 5–6 K. In the case of EPR measurements, the end of the smooth-wall waveguide (see Fig. 3) must be as closest as possible to the sample to avoid losses of scattered reflected waves. Since we are not interested in detecting the EPR signal, and, consequently, in the reflected microwaves, the waveguide is located about 7 mm above the sample, to allow for additional tolerance for the sample height and proper light beam alignment using the mirrors. Despite rather high losses of the reflected beam (17.8 dB in average in 325–500 GHz range, see Supplementary information), it is still possible to locate the EPR signal while calibrating the magnetic field sweep window. The whole space for the sample can be adjusted by manufacturing a different PCB (the diameter of PCB is 36 mm), while now the space is limited to 10 × 10 × 7 mm due to mirrors, temperature sensor, and the signal terminal alignment. The height of 7 mm is considered when the light excitation is not used, otherwise the sample height of 2–3 mm is recommended because of the required space for the light beam propagation. The microwave aperture is 5 mm in diameter. Depending on the sample's size, it can be arranged spatially on PCB in the way that the m.w. aperture and the light (spot of which is 2 × 3 mm) cover the dedicated area.

The EDMR signal and its stability directly depend on proper sample contact when exposed to cryogenic temperatures and high magnetic fields. The choice of contact type must be approached carefully depending on the sample itself, taking into account the above-mentioned conditions.

The best way to contact the sample is wire bonding with Au or Al wire which are "EPR-silent" materials. When the sample does not have deposited contact pads, one of the best solutions is to use conductive adhesive. We experimented with various conductive adhesives, and some of the carbon-based ones may introduce an unwanted EPR signal. As a result, we used the Ag-based paint, which demonstrated that it can be used even at liquid helium temperatures and provides excellent contact. In this work, the 15R SiC monocrystal was attached via Ag-based paint to the glass plate with deposited gold contact pads, which, in turn, was connected to the PCB board. All the signal wires were connected to the signal terminal, which also houses contacts for dedicated sensors.

IV. Results and Discussion

In this section, we present the results of 85–328.84-GHz EDMR experiments performed with the setup described above. We have performed the low-temperature multifrequency EPR and EDMR spectroscopy of 15R polytype SiC monocrystals

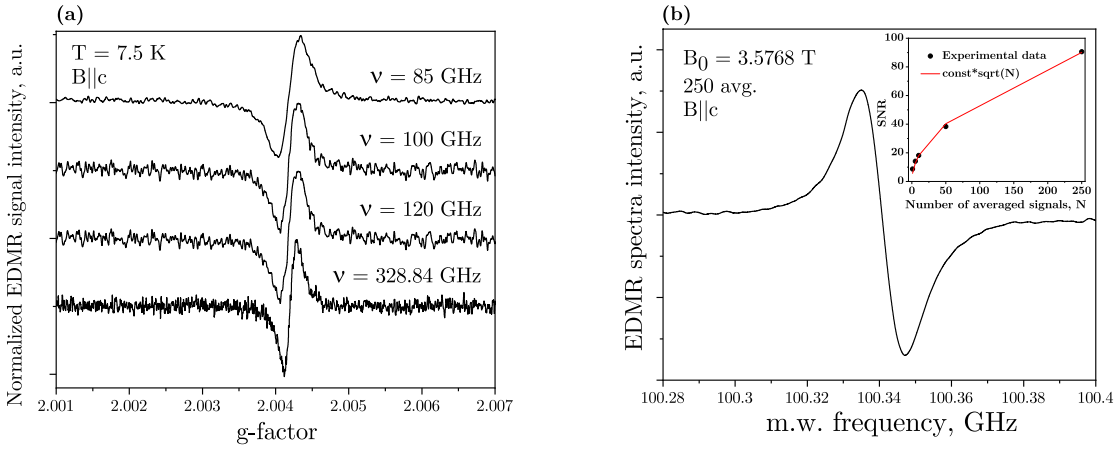

Fig. 4. (a) EDMR spectra measured in 15R SiC monocrystals with $(N_D - N_A) \approx 5 \times 10^{18}$ cm^{-3} at ν = 85–328.84 GHz, $B \| c$. The EDMR spectra were normalized to their maximum intensities. (b) FD EDMR spectra measured in 15R SiC monocrystals with $(N_D - N_A) \approx 5 \times 10^{18}$ cm^{-3} at ν = 100.28–100.4 GHz, B = 3.576891 T at T = 7.5 K, 250 averages, 2.048 s/sweep. The spectra were measured using magnetic field modulation at f_{mod} = 771 Hz with an amplitude of B_{mod} = 0.25 mT. The inner plot depicts the SNR to the number of averaged signals' dependence. Acquisition of a single MD sweep takes about the same time as an accumulation of 250 FD sweeps.

with $(N_D - N_A) \approx 5 \times 10^{18}$ cm^{-3} (where N_D is the donor concentration, N_A is the acceptor concentration). The monocrystals were grown by the modified Lely method [35]. The sample dimensions are 3.5 × 0.8 × 0.4 mm.

The EDMR measurements obtained at 85–328.84 GHz of 15R SiC monocrystal are shown in Fig. 4(a). In these monocrystals with $(N_D - N_A) \approx 5 \cdot 10^{18}$ cm^{-3}, the single line of the spin system S = 1/2 is present. The multifrequency measurements were made with a single spectrometer and two different m.w. sources. As shown in Fig. 4(a), the SNR at 85–120 GHz is 42, whereas at 328.84 GHz it is 29. We assume that this noticeable SNR difference is caused by m.w. sources' power variation and the EDMR spectra broadening. The output power to frequency dependence varies between m.w. sources. For example, an 80–120-GHz m.w. source has an output power of about 120 mW, whereas a 328.84-GHz source has only about 70 mW.

In terms of frequency-domain (FD) measurements, the THz FraScan setup can perform frequency sweeps while the magnetic field remains constant. The advantage of this technique is that it has a higher SNR and requires less measurement time than the magnetic field sweep. Fig. 4(b) depicts the frequency-domain EDMR (FD EDMR) spectra averaged 250 times with 2.048 s/sweep. The spectra of 250 averages were recorded in ∼8.5 min, while the magnetic field domain measurement takes about the same amount of time with the single sweep and twice lower SNR. Performing the signal averaging of the magnetic field sweep EDMR spectra using superconductive magnets has certain disadvantages, such as the magnetic field shift and noticeable magnet inertia. To suppress the latest one, the stabilization delay time must be set before recording a new spectra and the magnetic field ramping rate (to sweep the magnetic field up and down) has to be the same. In the case of FD measurements, the magnet is set to the persistent mode on the desired magnetic field value, which eliminates the problem described above.

Fig. 5(a) shows the m.w. power dependence of the EDMR signal intensity measured in 15R SiC monocrystals showing saturation above 40 mW. This power saturation effect takes place only when the incident m.w. power level is sufficient for populating the excited spin state of the spin system much faster than the system relaxes to its equilibrium population state due to the spin-lattice relaxation effects [36]. We can assume that the optimal minimum m.w. power required in such setups with nonresonant probe configuration to measure the magnetic field sweep EDMR begins at 20 mW. It should be noted that the power efficiency of the next in line m.w. source for the higher frequency (than reported here 328.84 GHz) of our setup (80–1100 GHz) is about ∼1% of the 80–120-GHz m.w. source.

Fig. 5(b) demonstrates the temperature dependence of EDMR spectra measured in 15R SiC monocrystals at ν = 100 GHz, showing that the EDMR spectra were observed at $T < 12$ K only. In general, the temperature dependence of an EDMR signal can give an information about the sample's recombination mechanisms and durability. We can assume that the signal disappears at $T > 12$ K because the hopping exchange interaction between nitrogen donors decreases.

The EDMR measurements under the light illumination with laser diodes of the 403–636.7-nm wavelength did not show any enhancement in the EDMR signal intensity.

It is well-known that in 15R SiC nitrogen N donors substitute five nonequivalent positions: three quasi-cubic "k_1," "k_2," and "k_3" (N_{k1}, N_{k2}, N_{k3}) and two hexagonal "h_1" and "h_2" (N_{h1}, N_{h2}) with donor energy levels in the band gap at ∼99 meV for $N_{k1,k2,k3}$ and ∼ 52 meV for $N_{h1,h2}$. As a result, the 15R SiC monocrystals with $(N_D - N_A) \approx 5 \times 10^{16}$ cm^{-3} reveal five triplet lines in the EPR spectra due to hyperfine interaction with ^{14}N nuclei (I = 1, nat. ab. 99.6%) related to the center with S = 1/2 [37], [38], [39]. The isolated N donors in 15R SiC have the following spin Hamiltonian parameters [38], [39].

1) N_{k1}: $g_\perp = 2.0026(2)$, $g_\parallel = 2.0040(2)$, $A_{iso} = A_\parallel = A_\perp = 33.6$ MHz.
2) N_{k2}: $g_\perp = 2.0030(2)$, $g_\parallel = 2.0037(2)$, $A_{iso} = 33.32$ MHz.
3) N_{k3}: $g_\perp = 2.0030(2)$, $g_\parallel = 2.0038(2)$, $A_{iso} = 30.36$ MHz.

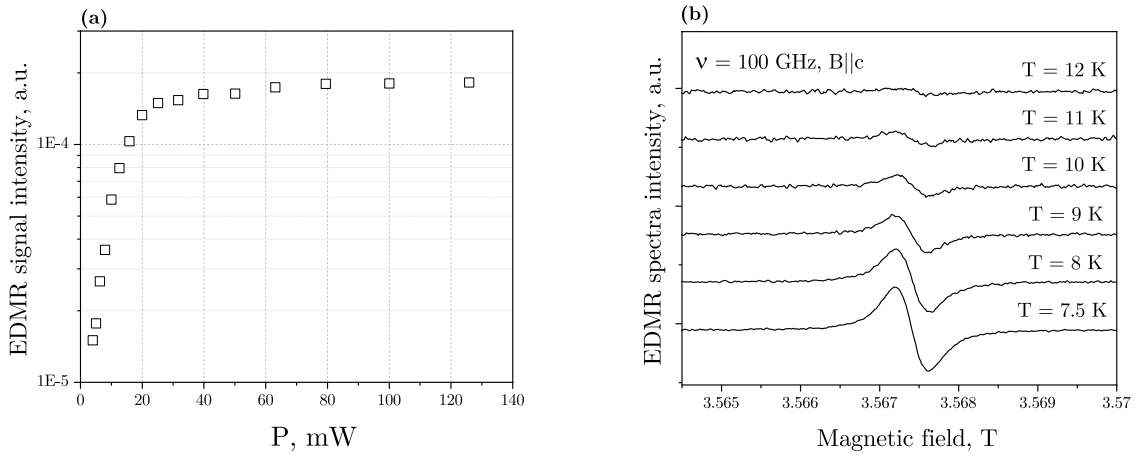

Fig. 5. m.w. power dependence of the EDMR signal intensity measured in 15R SiC monocrystals with $(N_D - N_A) \approx 5 \times 10^{18}$ cm^{-3}. $\nu = 100$ GHz and $T = 7.5$ K. (b) Temperature dependence of EDMR spectra measured in 15R SiC monocrystals with $(N_D - N_A) \approx 5 \times 10^{18}$ cm^{-3} at $\nu = 100$ GHz. The spectra were measured using magnetic field modulation at $f_{\text{mod}} = 771$ Hz with an amplitude of $B_{\text{mod}} = 0.25$ mT.

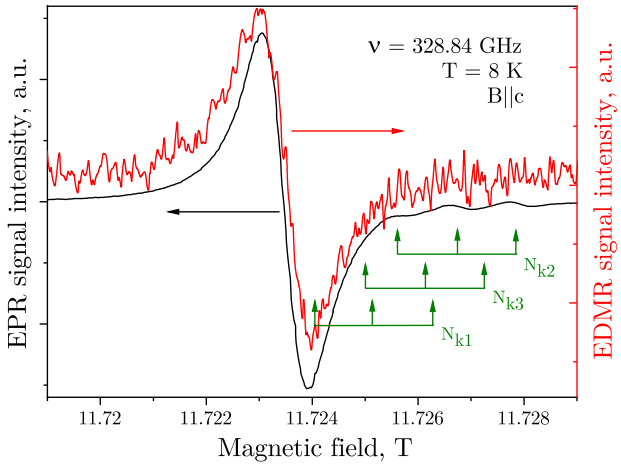

Fig. 6. EPR (black solid line) and EDMR (red solid line) spectra measured in 15R SiC monocrystals with $(N_D - N_A) \approx 5 \times 10^{18}$ cm^{-3}. $\nu = 328.84$ GHz and $T = 8$ K, $B \| c$. The EPR spectra were measured at $f_{\text{mod}} = 2.9$ kHz and EDMR spectra at $f_{\text{mod}} = 771$ Hz, both at $B_{\text{mod}} = 0.25$ mT.

4) N_{h1}: $g_\perp = 2.0028(2)$, $g_\parallel = 2.0035(2)$, $A_\perp \sim 1.1$ MHz, $A_\parallel \sim 2.1$ MHz.
5) N_{h2}: $g_\perp = 2.0023(2)$, $g_\parallel = 2.0031(2)$, $A_\perp \sim 1.4$ MHz, $A_\parallel \sim 2.2$ MHz.

From the EPR measurements at $\nu = 328.84$ GHz in both the orientations of the magnetic field with respect to the crystal c-axis, it was found that at $T < 20$ K, the 15R SiC samples reveal an intense line with $g_\perp = 2.0026(2)$ and $g_\parallel = 2.0043(2)$, and a line triplet of low intensity due to $N_{k1,k2,k3}$ donors. The EDMR spectra measured at $\nu = 328.84$ GHz and $T = 7.5$ K show a similar single line with $g_\perp = 2.0026(2)$ and $g_\parallel = 2.0043(2)$, and no traces of the N donors residing on the cubic sites were detected (see Fig. 6).

At $(N_D - N_A) \approx 5 \times 10^{18}$ cm^{-3}, the disappearance of $N_{h1,h2}$ donors having more shallow levels in the bandgap is expected along with the emergence of the single line due to exchange interaction between N donors.

In [40], the N atoms in the SiO_2–SiC interface regions of the n-channel lateral 4H SiC metal–oxide–semiconductor field-effect transistors (MOSFETs) were studied by low-temperature EDMR. The authors reported an intense EDMR signal at $T < 20$ K with C_{3V} symmetry having $g_\perp = 2.0008$ and $g_\parallel = 2.0047$ assigned to N donors residing hexagonal site in 4H SiC (N_h). However, from an earlier pulsed electron-nuclear double resonance (ENDOR) study of 4H SiC monocrystals with $(N_D - N_A) \approx 5 \times 10^{17}$ cm^{-3} [41], it was unambiguously proved that N_h donors in 4H SiC have $g_\perp = 2.0006(1)$ and $g_\parallel = 2.0065(1)$. At the same time, the high-field EPR study shows that no N_h line is observed in 4H SiC monocrystals with $(N_D - N_A) \approx 5 \times 10^{18}$ cm^{-3}, and the single line with $g_\perp = 2.0010(1)$ and $g_\parallel = 2.0054(1)$ [42] caused by the hopping exchange of a donor electron between N atoms at hexagonal and cubic positions appears [43]. Therefore, the EDMR signal observed in [40] should be attributed to the hopping exchange interaction of N donors residing at h and k positions in 4H SiC.

We assume that the same hopping conduction process between N donors is responsible for the appearance of the single line with $g_\perp = 2.0026(2)$ and $g_\parallel = 2.0043(2)$ in EPR and EDMR spectra of 15R SiC monocrystals with $(N_D - N_A) \approx 5 \times 10^{18}$ cm^{-3}. Therefore, we may suppose that the observed single line in EPR and EDMR spectra is caused by a spin-dependent hopping process due to the exchange interaction of N_{k1} and N_{h1} in 15R SiC. Measuring the EDMR spectra in the wide m.w. frequency range from 85 to 328.84 GHz allowed us to determine that no overlapping lines were hidden in the spectrum [see Fig. 4(a)]. A comprehensive EPR and EDMR study on spin dynamics of the exchange-coupled nitrogen donors in heavily doped n-type 15R SiC monocrystals can be found in [44]. In addition, more detailed information about the experimental setup can be found in [45].

V. Conclusion and Outlook

In this work, we showed the proof-of-concept of the EDMR setup based on the sub-THz FraScan spectrometer, its capabilities, and advantages. The advantages of using FD EDMR over MD EDMR result in higher SNR and lower measurement time consumption. The setup expands the range of measurement possibilities and paves the way for performing comprehensive EDMR studies. As the test samples in this setup, we used the 15R SiC monocrystals with a relatively

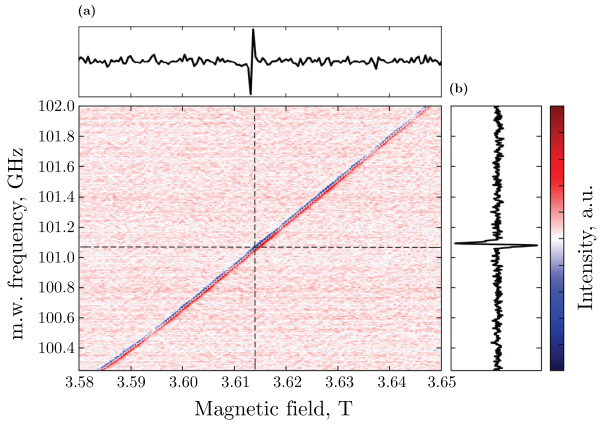

Fig. 7. Frequency-field map of EDMR spectra measured in 15R SiC monocrystals with $(N_D - N_A) \approx 5 \times 10^{18}$ cm^{-3} at $\nu = 100.2$–102 GHz, $B = 3.58$–3.65 T, and $T = 7.5$ K. Signal intensity values were omitted and shown in arbitrary units. The map resolution is 3000 per 219 points. Dashed lines correspond to a frequency and a magnetic field value of (a) and (b), respectively. (a) Single-frequency sweep spectra at $B = 3.615$ T. (b) Single magnetic field sweep spectra at $\nu = 101.14$ GHz. The map was recorded with the modulation frequency of $f_{\text{mod}} = 771$ Hz and with an amplitude of $B_{\text{mod}} = 0.25$ mT.

high donor concentration $(N_D - N_A) \approx 5 \times 10^{18}$ cm^{-3}, which revealed a single EPR and EDMR line at a low temperature with $g_\perp = 2.0026(2)$, $g_\parallel = 2.0043(2)$. This signal is, most probably, caused by a spin-dependent hopping process due to the exchange interaction of nitrogen donors residing on cubic k_1 and hexagonal h_1 nonequivalent positions in the 15R SiC lattice.

Regarding the prospects for the further EDMR technique development, we report on the first EDMR frequency-field map (EDMR FFM) of 15R SiC monocrystal recorded at $\nu = 100.2$–102 GHz, $B = 3.58$–3.65 T, and $T = 7.5$ K (see Fig. 7). The single-frequency sweep is 2.048-s long and the magnetic field sweep rate is 0.18 mT/s. The map contains 30 000 frequency scan points for each of the 219 steps of the magnetic field sweep.

From Fig. 7, we can see the straight line across the map, the behavior of which can be described by (1). Depending on the sample's defect complexity, these 2-D plots can qualitatively visualize recorded data in a wide range, helping to uniquely define the spin Hamiltonian parameters of high spin systems [17]. For instance, such plots can be useful when tracing the data of a frequency-dependent behavior of the sample's defect or viewing the zero-field splitting map.

Acknowledgment

The authors thank the whole research group of Prof. Patrick Lenahan (Pennsylvania State University, State College, PA, USA) and Dr. Boris Naydenov (Helmholtz-Zentrum Berlin, Berlin, Germany) for valuable discussion during the manuscript preparation.

References

[1] G. Kawachi, C. F. O. Graeff, M. S. Brandt, and M. Stutzmann, "Carrier transport in amorphous silicon-based thin-film transistors studied by spin-dependent transport," *Phys. Rev. B, Condens. Matter*, vol. 54, no. 11, pp. 7957–7964, Sep. 1996, doi: 10.1103/PhysRevB.54.7957.

[2] P. M. Lenahan and P. V. Dressendorfer, "Hole traps and trivalent silicon centers in metal/oxide/silicon devices," *J. Appl. Phys.*, vol. 55, no. 10, pp. 3495–3499, May 1984.

[3] P. M. Lenahan, J. J. Mele, J. F. Conley, R. K. Lowry, and D. Woodbury, "Predicting radiation response from process parameters: Verification of a physically based predictive model," *IEEE Trans. Nucl. Sci.*, vol. 46, no. 6, pp. 1534–1543, Dec. 1999.

[4] J. A. Weil and J. R. Bolton, *Basic Principles of Paramagnetic Resonance*. Hoboken, NJ, USA: Wiley, 2006, ch. 1, p. 16, doi: 10.1002/9780470084984.ch1.

[5] J.-M. Spaeth and H. Overhof, *Electrical Detection of Electron Paramagnetic Resonance*. Berlin, Germany: Springer, 2003, pp. 265–308, doi: 10.1007/978-3-642-55615-9_7.

[6] C. Boehme and H. Malissa, *Electrically Detected Magnetic Resonance Spectroscopy*. Hoboken, NJ, USA: Wiley, 2017, pp. 83–100, doi: 10.1002/9780470034590.emrstm1525.

[7] C. F. O. Graeff, G. Kawachi, M. S. Brandt, M. Stutzmann, and M. J. Powell, "Spin-dependent transport in amorphous silicon thin-film transistors," *J. Non-Crystalline Solids*, vols. 198–200, pp. 1117–1120, May 1996.

[8] M. I. G. Molina, "EPR-induced charge transport in highly doped crystalline n-type silicon carbide," Ph.D. dissertation, Dept. Phys., Paderborn Univ., Paderborn, Germany, 2000.

[9] J. Schmidt and I. Solomon, "Modulation de la photoconductivité dans le silicium á basse température par résonance magnetique électronique des impuretés peu profondes," *Compt. Rend.*, vol. 169, p. 263, Jan. 1966.

[10] D. J. Lepine, "Spin-dependent recombination on silicon surface," *Phys. Rev. B, Condens. Matter*, vol. 6, no. 2, pp. 436–441, Jul. 1972, doi: 10.1103/PhysRevB.6.436.

[11] D. Kaplan, I. Solomon, and N. F. Mott, "Explanation of the large spin-dependent recombination effect in semiconductors," *J. de Phys. Lettres*, vol. 39, no. 4, pp. 51–54, 1978, doi: 10.1051/jphyslet:0197800390405100.

[12] K. Fukuda and N. Asakawa, "Development of multi-frequency ESR/EDMR system using a rectangular cavity equipped with waveguide window," *Rev. Sci. Instrum.*, vol. 87, no. 11, Nov. 2016, Art. no. 113106, doi: 10.1063/1.4967712.

[13] W. Akhtar, A. Schnegg, S. Veber, C. Meier, M. Fehr, and K. Lips, "CW and pulsed electrically detected magnetic resonance spectroscopy at 263 GHz/12 T on operating amorphous silicon solar cells," *J. Magn. Reson.*, vol. 257, pp. 94–101, Aug. 2015. [Online]. Available: https://www.sciencedirect.com/science/article/pii/S1090780715001299

[14] V. Lang et al., "Electrically detected magnetic resonance in a W-band microwave cavity," *Rev. Sci. Instrum.*, vol. 82, no. 3, Mar. 2011, Art. no. 034704, doi: 10.1063/1.3557395.

[15] A. Sojka et al., "Sample holders for sub-THz electron spin resonance spectroscopy," *IEEE Trans. Instrum. Meas.*, vol. 71, pp. 1–12, 2022.

[16] P. Neugebauer et al., "Ultra-broadband EPR spectroscopy in field and frequency domains," *Phys. Chem. Chem. Phys.*, vol. 20, no. 22, pp. 15528–15534, 2018, doi: 10.1039/C7CP07443C.

[17] A. Sojka, M. Šedivý, O. Laguta, A. Marko, V. Santana, and P. Neugebauer, "High-frequency EPR: Current state and perspectives," *Electron Paramagn. Reson.*, vol. 27, pp. 214–252, Nov. 2021, doi: 10.1039/9781839162534-00214.

[18] M. Algasinger et al., "Improved black silicon for photovoltaic applications," *Adv. Energy Mater.*, vol. 3, no. 8, pp. 1068–1074, Aug. 2013, doi: 10.1002/aenm.201201038.

[19] D. J. McCrory et al., "Slow- and rapid-scan frequency-swept electrically detected magnetic resonance of MOSFETs with a non-resonant microwave probe within a semiconductor wafer-probing station," *Rev. Sci. Instrum.*, vol. 90, no. 1, Jan. 2019, Art. no. 014708, doi: 10.1063/1.5053665.

[20] J. P. Ashton, B. R. Manning, W. R. Barker, and P. M. Lenahan, "Ultra-low field frequency-swept electrically detected magnetic resonance," *J. Appl. Phys.*, vol. 129, no. 8, Feb. 2021, Art. no. 083903, doi: 10.1063/5.0042484.

[21] D. J. McCrory et al., "Wafer-level electrically detected magnetic resonance: Magnetic resonance in a probing station," *IEEE Trans. Device Mater. Rel.*, vol. 18, no. 2, pp. 139–143, Jun. 2018.

[22] J. P. Ashton and P. M. Lenahan, "Multiple-photon transitions in electrically detected magnetic resonance measurements of 4H-SiC transistors," *Phys. Rev. B, Condens. Matter*, vol. 102, no. 2, Jul. 2020, Art. no. 020101, doi: 10.1103/PhysRevB.102.020101.

[23] A. R. Stegner, C. Boehme, H. Huebl, M. Stutzmann, K. Lips, and M. S. Brandt, "Electrical detection of coherent 31P spin quantum states," *Nature Phys.*, vol. 2, no. 12, pp. 835–838, Dec. 2006, doi: 10.1038/nphys465.

[24] H. Morishita et al., "Linewidth of low-field electrically detected magnetic resonance of phosphorus in isotopically controlled silicon," *Appl. Phys. Exp.*, vol. 4, no. 2, Jan. 2011, Art. no. 021302, doi: 10.1143/apex.4.021302.

[25] D. R. McCamey, J. Van Tol, G. W. Morley, and C. Boehme, "Electronic spin storage in an electrically readable nuclear spin memory with a lifetime >100 seconds," *Science*, vol. 330, no. 6011, pp. 1652–1656, Dec. 2010, doi: 10.1126/science.1197931.

[26] M. Xiao, I. Martin, E. Yablonovitch, and H. W. Jiang, "Electrical detection of the spin resonance of a single electron in a silicon field-effect transistor," *Nature*, vol. 430, no. 6998, pp. 435–439, Jul. 2004, doi: 10.1038/nature02727.

[27] M. A. Anders, P. M. Lenahan, C. J. Cochrane, and J. van Tol, "Physical nature of electrically detected magnetic resonance through spin dependent trap assisted tunneling in insulators," *J. Appl. Phys.*, vol. 124, no. 21, Dec. 2018, Art. no. 215105, doi: 10.1063/1.5057354.

[28] G. W. Morley, L.-C. Brunel, and J. van Tol, "A multifrequency high-field pulsed electron paramagnetic resonance/electron-nuclear double resonance spectrometer," *Rev. Sci. Instrum.*, vol. 79, no. 6, Jun. 2008, Art. no. 064703, doi: 10.1063/1.2937630.

[29] C. Meier et al., "Multi-frequency EDMR applied to microcrystalline thin-film silicon solar cells," *J. Magn. Reson.*, vol. 234, pp. 1–9, Sep. 2013. [Online]. Available: https://www.sciencedirect.com/science/article/pii/S1090780713001407

[30] A. Schnegg, J. Behrends, M. Fehr, and K. Lips, "Pulsed electrically detected magnetic resonance for thin film silicon and organic solar cells," *Phys. Chem. Chem. Phys.*, vol. 14, no. 12, pp. 14418–14438, 2012, doi: 10.1039/C2CP41258F.

[31] F. V. Sharov, S. J. Moxim, G. S. Haase, D. R. Hughart, and P. M. Lenahan, "A comparison of radiation-induced and high-field electrically stress-induced interface defects in Si/SiO_2 MOSFETs via electrically detected magnetic resonance," *IEEE Trans. Nucl. Sci.*, vol. 69, no. 3, pp. 208–215, Mar. 2022.

[32] A. K. Hassan et al., "Ultrawide band multifrequency high-field EMR technique: A methodology for increasing spectroscopic information," *J. Magn. Reson.*, vol. 142, no. 2, pp. 300–312, Feb. 2000. [Online]. Available: https://www.sciencedirect.com/science/article/pii/S1090780799919523

[33] G. W. Morley, D. R. McCamey, H. A. Seipel, L.-C. Brunel, J. van Tol, and C. Boehme, "Long-lived spin coherence in silicon with an electrical spin trap readout," *Phys. Rev. Lett.*, vol. 101, no. 20, Nov. 2008, Art. no. 207602, doi: 10.1103/PhysRevLett.101.207602.

[34] J. Grutzner, "Nuclear magnetic resonance spectroscopy | principles," in *Encyclopedia of Analytical Science*, 2nd ed, P. Worsfold, A. Townshend, and C. Poole, Eds. Oxford, U.K.: Elsevier, 2005, pp. 211–237. [Online]. Available: https://www.sciencedirect.com/science/article/pii/B0123693977004052

[35] Y. M. Tairov and V. F. Tsvetkov, "Investigation of growth processes of ingots of silicon carbide single crystals," *J. Cryst. Growth*, vol. 43, no. 2, pp. 209–212, Mar. 1978. [Online]. Available: https://www.sciencedirect.com/science/article/pii/0022024878901690

[36] C. P. Poole and H. A. Farach, *Theory of Magnetic Resonance*, 2nd ed. New York, NY, USA: Wiley-Interscience, 1987.

[37] W. Götz et al., "Nitrogen donors in 4H-silicon carbide," *J. Appl. Phys.*, vol. 73, no. 7, pp. 3332–3338, Apr. 1993, doi: 10.1063/1.352983.

[38] E. N. Kalabukhova, N. N. Kabdin, S. N. Lukin, E. N. Mokhov, and B. D. Shanina, "ESR spectra of nonequivalent nitrogen sites in 15R SiC," *Sov. Phys. Solid State*, vol. 31, no. 3, p. 378, 1989.

[39] D. Savchenko et al., "EPR, ESE, and pulsed ENDOR study of the nitrogen donors in 15R SiC grown under carbon-rich conditions," *Phys. Status Solidi B*, vol. 252, no. 3, pp. 566–572, Mar. 2015, doi: 10.1002/pssb.201451452.

[40] T. Umeda et al., "Behavior of nitrogen atoms in $SiC-SiO_2$ interfaces studied by electrically detected magnetic resonance," *Appl. Phys. Lett.*, vol. 99, no. 14, Oct. 2011, Art. no. 142105, doi: 10.1063/1.3644156.

[41] E. N. Kalabukhova et al., "EPR, ESE and pulsed ENDOR study of nitrogen related centers in 4H-SiC wafers grown by different technologies," *Mater. Sci. Forum*, vols. 556–557, pp. 355–358, Sep. 2007.

[42] U. Gerstmann et al., "Nitrogen donor aggregation in 4H-SiC: G-Tensor calculations," *Mater. Sci. Forum*, vols. 556–557, pp. 391–394, Sep. 2007.

[43] E. N. Kalabukhova, S. N. Lukin, B. D. Shanina, L. V. Artamonov, and E. N. Mokhov, "Hopping conduction effects in the ESR spectra of heavily nitrogen-doped 4H SiC," *Sov. Phys. Solid State*, vol. 32, no. 3, p. 482, 1990.

[44] A. Solodovnyk et al., "Spin dynamics of exchange-coupled nitrogen donors in heavily doped n -type 15R SiC monocrystals: Multifrequency EPR and EDMR study," *Phys. Rev. B*, vol. 107, no. 15, Apr. 2023, Art. no. 155202, doi: 10.1103/PhysRevB.107.155202.

[45] A. Solodovnyk, "Magneto optical studies of solid states materials," Ph.D. dissertation, Central Eur. Inst. Technol., Res. Inst., Brno Univ. Technol., Brno, Czech Republic, 2022. [Online]. Available: https://www.vut.cz/studenti/zav-prace/detail/150142

Artur Solodovnyk received the bachelor's and master's degrees from the Taras Shevchenko National University of Kyiv, Kyiv, Ukraine, in 2015 and 2017, respectively. He is currently pursuing the Ph.D. degree with the Magneto-Optical and Terahertz Spectroscopy (MOTeS) Group, Central European Institute of Technology, Brno University of Technology (BUT), Brno, Czech Republic, under the supervision of Petr Neugebauer.

His research interests include the study of defects in semiconductor materials using electrically detected magnetic resonance (EDMR).

Dariya Savchenko received the Ph.D. and Dr.Sc. degrees in physics and mathematics from the V. E. Lashkaryov Institute of Semiconductor Physics, National Academy of Sciences (NAS) of Ukraine, Kyiv, Ukraine, in 2010 and 2019, respectively.

She is currently the Scientist with the Department of Analysis of Functional Materials, Institute of Physics, Czech Academy of Sciences (CAS), Prague, Czech Republic, and an Associate Professor with the Department of General Physics and Modeling of Physical Processes, National Technical University of Ukraine "Igor Sikorsky Kyiv Polytechnic Institute," Kyiv. She has authored or coauthored more than 165 papers published in international journals and conference proceedings. Her research interests include magnetic resonance study in semiconductors, dielectrics, and biomaterials by continuous wave and pulsed electron paramagnetic resonance (EPR) spectroscopy methods.

Dr. Savchenko is a member of IEEE Magnetics Society.

Oleksii Laguta received the Ph.D. degree in lasers, molecules, atmospheric radiation from the University of Lille, Lille, France, in 2016.

After that, he spent 18 months working on the development of frequency-domain rapid-scan high-frequency electron paramagnetic resonance (HF-EPR) as a Post-Doctoral Research Fellow in the group of Petr Neugebauer (AG van Slageren, Stuttgart University, Stuttgart, Germany). Since 2019, he has been a Junior Researcher with the Central European Institute of Technology, Brno University of Technology, Brno, Czech Republic. He currently studies the electron spin dynamics at high magnetic fields using the rapid-scan electron paramagnetic resonance (EPR) spectroscopy.

Petr Neugebauer received the Ph.D. degree in physics of condensed matter and radiation from the Grenoble High Magnetic Field Laboratory (GHMFL), Grenoble, France, in 2010.

After his two years of post-doctoral stay in the research group of Prof. T. Prisner at the Center for Biomolecular Magnetic Resonance, Goethe University, Frankfurt, Germany, he joined the research group of Prof. J. van Slageren at the University of Stuttgart, Stuttgart, Germany. He is currently the Group Leader and the Founder of the Magneto-Optical and Terahertz Spectroscopy (MOTeS) Group, Central European Institute of Technology (CEITEC), Brno University of Technology (BUT), Brno, Czech Republic. The group focuses on the development of high-frequency electron paramagnetic resonance (HF-EPR) spectroscopy, especially frequency rapid scan above 100 GHz (ERC grant), HF-EPR applications to molecular magnetism, thin films, and molecular materials.

Dr. Neugebauer has received the Marie Curie Fellowship during his Ph.D. degree.